# AhpF Can Be Dissected into Two Functional Units: Tandem Repeats of Two Thioredoxin-like Folds in the N-Terminus Mediate Electron Transfer from the Thioredoxin Reductase-like C-Terminus to AhpC†

Leslie B. Poole,*,‡ Adam Godzik,§ Akbar Nayeem,|| and Jeffrey D. Schmitt‡,⊥

*Department of Biochemistry, Wake Forest University School of Medicine, Winston-Salem, North Carolina 27157, The Burnham Institute, 10901 North Torrey Pines Road, La Jolla, California 92037, Tripos Associates, Inc., St. Louis, Missouri 63144-2913, and Targacept, Inc., P.O. Box 1487,Winston-Salem, North Carolina 27102*

*Received February 22, 2000; Revised Manuscript Received April 3, 2000*

ABSTRACT: AhpF, the flavin-containing component of the *Salmonella typhimurium* alkyl hydroperoxide reductase system, catalyzes the NADH-dependent reduction of an active-site disulfide bond in the other component, AhpC, which in turn reduces hydroperoxide substrates. The amino acid sequence of the C-terminus of AhpF is 35% identical to that of thioredoxin reductase (TrR) from *Escherichia coli*. AhpF contains an additional 200-residue N-terminal domain possessing a second redox-active disulfide center also required for AhpC reduction. Our studies indicate that this N-terminus contains a tandem repeat of two thioredoxin (Tr)-like folds, the second of which contains the disulfide redox center. Structural and catalytic properties of independently expressed fragments of AhpF corresponding to the TrR-like C-terminus (F[208−521]) and the 2Tr-like N-terminal domain (F[1−202]) have been addressed. Enzymatic assays, reductive titrations, and circular dichroism studies of the fragments indicate that each folds properly and retains many functional properties. Electron transfer between F[208−521] and F[1−202] is, however, relatively slow ($4 \times 10^4$ $M^{-1}$ $s^{-1}$ at 25 °C) and nonsaturable up to 100 $\mu$M F[1−202]. TrR is nearly as efficient at F[1−202] reduction as is F[208−521], although neither the latter fragment, nor intact AhpF, can reduce Tr. An engineered mutant AhpC substrate with a fluorophore attached via a disulfide bond has been used to demonstrate that only F[1−202], and not F[208−521], is capable of electron transfer to AhpC, thereby establishing the direct role this N-terminal domain plays in mediating electron transfer between the TrR-like part of AhpF and AhpC.

The alkyl hydroperoxide reductase system of *Salmonella typhimurium* catalyzes the NADH-dependent reduction of organic hydroperoxides and hydrogen peroxide through action of a 57 kDa FAD-containing protein, AhpF, and a 21 kDa protein, AhpC (a member of the peroxiredoxin family) (*1*, *2*). Reductive titrations, catalytic effects of thiol-modifying agents, and functional studies of cysteine-to-serine mutants of both proteins strongly support a flavin and redox-active cystine-based mechanism involving AhpF-mediated transfer of electrons between reduced pyridine nucleotides and AhpC, followed by the reduction of peroxides by the nascent thiol groups of AhpC (*2*−*5*). Amino acid sequence comparisons have demonstrated homology between the C-terminal-most 314 amino acids of AhpF and the 35 kDa flavoprotein thioredoxin reductase (TrR)[1] from *Escherichia coli*; the catalytic half-cystine residues of TrR (Cys135 and Cys138) are conserved in AhpF as Cys345 and Cys348 (*6*, *7*). The N-terminal region of approximately 200 amino acids in AhpF is absent from TrR and aligns well only with corresponding regions of AhpF homologues from other bacteria (*6*); the N-terminus contains a second redox-active disulfide bond between Cys129 and Cys132 (*3*). Both redox-active disulfide centers are essential for catalysis (*5*).

AhpF, like TrR, is classified as a pyridine nucleotide: disulfide oxidoreductase within a subclass distinct from that exemplified by the well-characterized flavoprotein glutathione reductase (*8*). Initial indications of these differences shown by active-site peptide comparisons and sequence alignments have been borne out by structural determinations for TrR as compared with those for glutathione reductase,

† This work was supported by grants from the National Institutes of Health (GM50389) and The Council for Tobacco Research, Inc. (SA006 and 4501), computing time from the North Carolina Supercomputing Center to L.B.P, and NIH grant GM60049 to A.G.

* Corresponding author: Department of Biochemistry, Wake Forest University School of Medicine, Medical Center Blvd., Winston-Salem, NC 27157; tel no. 336-716-6711; fax no. 336-716-7671; E-mail lbpoole@wfubmc.edu; URL http://www.wfubmc.edu/biochem/faculty/Poole/poole.html.

‡ Department of Biochemistry, Wake Forest University School of Medicine.

§ Bioinformatics and Biological Complexity Program, The Burnham Institute.

|| Tripos Associates, Inc.

⊥ Targacept, Inc.

[1] Abbreviations used: TrR, thioredoxin reductase; Tr, thioredoxin; F[1−202], truncated AhpF including residues 1 through 202; F[208−521], truncated AhpF including methionine plus residues 208 through 521; DMSO, dimethyl sulfoxide; DTNB, 5,5′-dithiobis(2-nitrobenzoic acid); TNB, 5-thio-2-nitrobenzoic acid; IPTG, isopropyl $\beta$-D-thiogalactopyranoside; AhpC-FAM, carboxyfluorescein attached through a linker and a disulfide bond to Cys165 of the C46S mutant of AhpC.; FAM-SE, 5-(and 6-)carboxyfluorescein, succinimidyl ester; AEMTS, 2-aminoethyl methanethiosulfonate; CD, circular dichroism; FFAS, fold and function assignment system; $EH_2$, two-electron-reduced enzyme; $EH_4$, four-electron-reduced enzyme; $EH_6$, six-electron-reduced enzyme.

10.1021/bi000405w CCC: $19.00 
Published on Web 05/05/2000

trypanothione reductase, mercuric reductase, lipoamide dehydrogenase, and NADH peroxidase (*9, 10*). TrR and AhpF are missing the C-terminal-most interface domain necessary for subunit interactions within these other enzymes and have their cystine disulfide redox centers (with cysteinyl residues separated by two rather than four amino acids) within their pyridine nucleotide- rather than FAD-binding domains (*7, 10, 11*). This alteration in architecture has significant implications for the catalytic mechanisms of these enzymes; both the pyridine nucleotide and disulfide centers of TrR must interact with the *re* face of the flavin isoalloxazine ring (*8*). Furthermore, the nascent dithiol of TrR generated by electron transfer from the flavin must subsequently interact with its relatively large protein substrate, thioredoxin (Tr). X-ray crystallographic analyses of TrR have allowed for the characterization of a form of the enzyme in which the CXXC redox center is in close proximity to the isoalloxazine ring (3.0 and 4.8 Å from the C4a atom of the FAD for the sulfur atoms of Cys138 and Cys135, respectively) and the nicotinamide ring of $NADP^+$ is distant from the flavin (>17 Å) (*9*). An alternative conformation of the enzyme, with the isoalloxazine and nicotinamide rings proximal and the disulfide/dithiol center rotated to a more exposed position, was initially proposed on the basis of structural considerations (*8, 9*); indirect evidence for this putative conformational change during catalysis has been obtained by several approaches (*12*−*15*).

Consideration of the structural bases for AhpF catalysis also presents a good case for conformational fluctuations during catalysis (*3, 16*). At the least, electrons must pass from NADH to FAD, then to the TrR-like redox disulfide center (Cys345−Cys348), and on to the large AhpC substrate. In addition, the disulfide redox center in the N-terminus of AhpF (Cys129−Cys132) is required for AhpC reduction; our working model of the catalytic cycle therefore includes an intermediary step of electron transfer through Cys129−Cys132 of AhpF before transfer to AhpC (*3, 5, 16*). Given the multiple domain interactions expected to occur, we set out to characterize biochemical and structural aspects of these interactions through separate expression of the TrR-like C-terminal part of AhpF (F[208−521]) and the "appended" N-terminal part of AhpF (F[1−202]).[2] Our primary goals for this project were (i) to test the hypothesis that the N-terminus of AhpF is the direct electron donor to AhpC, (ii) to distinguish between intra- and intermolecular electron-transfer events involved in catalysis by AhpF, (iii) to identify the oligomerization state of each fragment and intact AhpF and localize the site(s) of putative subunit interactions, and (iv) to pursue independent modeling of separate parts of the polypeptide, if appropriate.

Our results, reported herein, have established that the N-terminal disulfide center of AhpF mediates electron transfer to AhpC. Furthermore, it is now clear that interdomain electron transfers in AhpF occur within, rather than between, molecules of this dimeric enzyme and may occur between domains in different subunits of the dimer.

[2] F[208−521] was designed on the basis of sequence alignment results between AhpF and TrR, where the region in common begins with residue 208 of AhpF (and residue 1 of TrR). F[1−202] was designed on the basis of previous limited tryptic digests which yield an intact C-terminal fragment starting at residue 203.

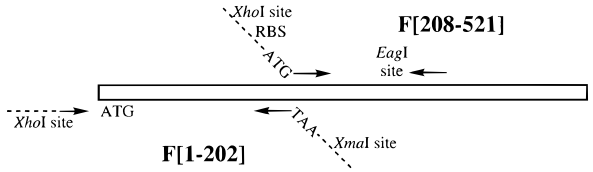


FIGURE 1: Generation of expression plasmids for F[1−202] and F[208−521] using PCR amplification. Reactions with the primers and the wild-type *ahpF* gene as template were carried out as described in Experimental Procedures.

## EXPERIMENTAL PROCEDURES

*Materials*. NADH and NADPH were purchased from Boehringer-Mannheim. Sigma was the supplier for dimethyl sulfoxide (DMSO), methyl viologen, cumene hydroperoxide, molecular biology-grade ammonium sulfate, and bovine pancreas insulin. DTNB, dithiothreitol, and most reagents used for buffers and protein gels were obtained from Research Organics, Inc. Bacteriological media components were purchased from Fisher. Restriction endonucleases and DNA-modifying enzymes were purchased from either New England Biolabs or Promega and were used as recommended by the supplier.

*Mutagenesis and Protein Purification Methods*. Plasmids for expressing AhpF mutant proteins truncated at the N-terminus (F[208−521]) or the C-terminus (F[1−202]) were generated by PCR amplification of the region of interest as shown in Figure 1(pAF1 and pOXO4 plasmids have been described earlier) (*2*). To generate plasmid pAF[208−521] for expression of the C-terminal fragment of AhpF, the forward primer (CCGG*CTCGAG*GAGGTGAAAAAAAAT-GAACAAACGCGATGCG) was designed to introduce new *Xho*I (italics) and ribosome-binding (underlined) sites, nine intervening residues, a new ATG codon, and then 15 residues of sequence matching codons 208−212 of AhpF. The reverse primer was an 18-mer which matched sequence complementary to codons 370− 375 of *ahpF*. The PCR reaction mixture contained 1 $\mu$g of pAF1 plasmid linearized with *Xho*I, 50 nM of forward and reverse primers, 250 $\mu$M dNTPs, 0.5 unit of *Taq* polymerase and diluted buffer from Promega, and 2.5 mM additional $MgCl_2$ in a total volume of 50 $\mu$L. Thirty cycles total (1 min at 94 °C, 2 min at 55 °C, and 2 min at 72 °C) were carried out after addition of the enzyme during preincubation at 94 °C. The appropriate-sized (approximately 500 bp) PCR fragment was excised from a 1% agarose gel and purified by GeneClean (Bio101). Isolated PCR fragment and pAF1 were digested with *Xho*I and *Eag*I; restriction enzymes added to the PCR fragment were inactivated (65 °C for 20 min) prior to ligation, and the 3.1 kb fragment of pAF1 was isolated from a 1% agarose gel by GeneClean (Bio101). The pAF[208−521] plasmid was isolated from a single colony using Promega Wizard preps following overnight ligation at 15 °C, transformation into XL1-Blue cells, and growth on LB-cam plates, and the sequence of the engineered fragment was confirmed in its entirety (Sequenase kit, Version 2.0, from United States Biochemicals). Generation of the pAF[1−202] plasmid followed a very similar strategy, but the entire fragment was generated by PCR (forward primer, TAATACGACT-CACTATAGGG; reverse primer, CCC*CCCGGG*TTA-GCGTTTTTCTGC, introducing a new stop codon after codon 202, underlined, and an *Xma*I site, in italics) using

the following modifications: pAF1 template was first linearized with *Nde*I, PCR reactions included dNTPs at 400 $\mu$M and Vent polymerase from New England Biolabs with the corresponding buffer (100 $\mu$L total), all reactions during the 35 cycles were for 1 min each with the extension reaction at 50 °C, and the product was about 800 bp. The *Xma*I- and *Xho*I-digested PCR fragment was ligated into similarly digested pOXO4 vector pretreated with calf-intestinal phosphatase (2 units at 37 °C for 30 min) following isolation of each with GeneClean.

Sequences of the PCR-generated regions of each expression plasmid were confirmed in their entirety using the Sequenase 2.0 kit from US Biochemicals and/or analyses carried out by the DNA sequence analysis core laboratory of the Comprehensive Cancer Center of Wake Forest University using an Applied Biosystems, Inc. Prism 377 automated DNA sequencer. The standard buffer for most protein procedures was 25 mM potassium phosphate at pH 7.0; all buffers for proteins contained 1 mM EDTA unless stated otherwise. Purification of the F[208−521] mutant from IPTG-induced JM109(DE3) cultures followed procedures very similar to those described for wild-type AhpF (*2*), except that the DE52 column was preequilibrated in 10 mM potassium phosphate buffer and eluted with a gradient from 10 to 60 mM potassium phosphate (F[208−521] elutes at lower ionic strength than intact AhpF). F[1−202] was purified in a manner similar to that used for F[208−521] using a DE52 or Q Sepharose column preequilibrated with 5 mM potassium phosphate and eluted with a gradient from 5 to 65 mM of the buffer. A BioGel A 0.5-m column was used for additional purification where necessary. Eight liters of bacterial culture yielded 350 mg of pure F[1−202] protein. Wild-type and C129,132S AhpF as well as AhpC from *S. typhimurium* were expressed and purified as described previously (*2, 5*).

TrR and thioredoxin (Tr) used in assays to determine the substrate specificity of F[208−521] were gifts from Dr. Charles Williams, Jr., of the University of Michigan. TrR used in DTNB-linked F[1−202] reductase assays was expressed and purified in our laboratory as follows. PCR primers (CCG*GAATTC*AGGAGGAAGTATA-GATGGGCACGACCAAACAC and CC*AAGCTT*T-TATTTTGCGTCAGCTAAACC) designed to introduce *Eco*RI and *Hin*dIII sites (in italics) at the beginning and end, respectively, of the structural gene were used to amplify *trxB* present on pDG026, an *lrp*- and *trxB*-containing plasmid supplied by Dr. Ian Blomfield (*17*); the PCR method was similar to that described to create pAF[208−521] (above). Subcloning of the *Eco*RI-*Hin*dIII fragment into the ampicillin-resistant expression vector pPROK-1 (Clontech) also followed procedures similar to those described for pAF[208−521], except that an intermediate clone of the *trxB* gene in the TA-cloning vector pCR2.1 (Invitrogen) was generated, and both the *trxB* and pPROK-1 *Eco*RI-*Hin*dIII fragments were isolated by GeneClean from a 0.8% agarose gel prior to ligation. The new expression vector, pTrR, was verified by full sequencing of the insert. For purification of TrR, cultures of *E. coli* strain XL1-Blue harboring pTrR were grown in 10 L of ampicillin-containing Luria Bertani broth after inoculation to 2% from an overnight culture. IPTG was added to 0.4 mM when the culture reached an $A_{600}$ of 1.4, and growth was continued overnight. Isolation of the protein proceeded as described previously for AhpF using DE52 and AffiGel Blue columns (*2*), except that the DE52 column was washed with 80 mM potassium phosphate buffer and eluted with a linear gradient from 80 to 160 mM potassium phosphate.

*Spectroscopic Methods.* Assays and titrations were carried out at 25 °C. UV−visible absorbance spectra were recorded using a Milton Roy Spectronic 3000 diode array spectrophotometer with 0.35 nm resolution; single-wavelength data were obtained with a Gilford 220 recording spectrophotometer or with an Applied Photophysics DX.17 MV stopped-flow spectrofluorometer. Circular dichroism (CD) spectra were recorded with a Jasco J-720 spectropolarimeter. Estimation of secondary-structure content from CD spectra was carried out using two programs, Varslc1 (*18*) and Selcon (*19*), available from Jasco within their Softsec program (either two or six proteins were excluded with each iteration for Varslc1, and the Kabsch and Sander calculation of the secondary structure data for reference proteins was used for Selcon). Catalytic assays, thiol content assays using DTNB, microbiuret assays to determine protein content, and analyses of flavin content were all carried out as previously described (*2, 3*). TrR activity was measured using both DTNB- and insulin-linked assays (*20, 21*). Spectrophotometric titrations were conducted under anaerobic conditions using a glass titration cuvette assembly, an oxygen-scrubbing system for NADH titrations, and methyl viologen added to solutions undergoing dithionite titrations, as outlined previously (*3*).

*Synthesis of AhpC-FAM.* A new AhpC substrate, AhpC-FAM, was engineered by attaching a fluorescein derivative, via a disulfide bond, to the single cysteine of the C46S mutant of AhpC (*4*) by the following method. Carboxyfluorescein succinimidyl ester (FAM-SE; 5- and 6-isomers from Molecular Probes; 56 $\mu$mol predissolved in DMSO) was incubated at room temperature for 2−3 h with 2-aminoethyl methanethiosulfonate (AEMTS from Anatrace; 37.5 $\mu$mol predissolved in DMSO) in a volume of 2.5 mL containing 60 mM sodium bicarbonate and 71% DMSO. To block excess amine-reactive FAM-SE, the reagent mixture was further incubated overnight at 4 °C with 120 $\mu$mol of glycine. Thiol reactivity of the putative carboxyfluorescein-linked AEMTS was assessed by titration of TNB (generated through addition of dithiothreitol to a slight excess of DTNB) with this reagent and observation of changes in $A_{412}$. A 2-fold molar excess of the reagent was then incubated with 6 $\mu$mol of C46S AhpC in the standard buffer (DMSO at about 21% after mixing) for 10 min at room temperature followed by gel filtration chromatography on a G-50 Sephadex column to remove excess reagent. Modified protein concentration was assessed by the microbiuret assay (*22*) and the Bradford assay (using reagents from BioRad) (*23*) with bovine serum albumin as the standard. Fluorescence measurements using an SLM Aminco Bowman Series 2 luminescence spectrophotometer indicated a 70% decrease in fluorescence of the bound fluorescein ($\lambda_{max,ex} = 498$ nm, $\lambda_{max,em} = 522$ nm; $\epsilon_{495} \sim 40\,000$ M$^{-1}$ cm$^{-1}$). Assays of AhpC-FAM with 0.06 $\mu$M intact AhpF or 0.6 $\mu$M F[208−521] were carried out aerobically on the stopped-flow spectrophotometer using 150 $\mu$M NADH, 0−72 $\mu$M AhpC-FAM, and standard peroxidase assay buffer (but no peroxide); rates were assessed for absorbance changes at 340 nm and for fluorescence changes using excitation at 493 nm and a 510 nm filter. Rates of

fluorescence changes were directly proportional to rates of absorbance changes up to 29 $\mu$M AhpC-FAM. F[1−202], which is not reducible with NADH, was incubated overnight at 4 °C with a 100-fold excess of dithiothreitol and reisolated by gel filtration chromatography on a G-50 Sephadex column prior to assay with AhpC-FAM.

*Analytical Ultracentrifugation.* Sedimentation equilibrium analyses were performed using an Optima XL-A analytical ultracentrifuge (Beckman Instruments, Palo Alto, CA) equipped with absorbance optics and an An60 Ti rotor. Data for AhpF, F[1−202], and F[208−521], in 50 mM potassium phosphate buffer at pH 7.0 containing 100 mM NaCl were collected in two independent runs with each protein at 2−3 concentrations and 3−4 speeds each time. Concentrations were varied from 3 to 94 $\mu$M for intact AhpF and F[208−521], and from 19 to 130 $\mu$M for F[1−202], with 110 $\mu$L of each sample loaded into three of the six sectors of each cell and buffer loaded into the reference sectors. Samples were brought to rotor speeds of 6 000−14 300 rpm for intact AhpF and F[208−521] or 12 000−22 000 rpm for F[1−202] and allowed to equilibrate at 20 °C for 12, 14, and 16 h, and then cells were scanned at 280 and 450 nm for the flavoproteins and 279 nm for F[1−202]. Scans were performed with a radial step size of 0.001 cm and were the average of five replicates. In each case, scans were performed after 4 h at 40 000 rpm to measure the baseline by meniscus depletion (*24*). Global analysis of multiple data sets was performed using the Windows version of NONLIN (*25*). Only data at less than 1.45 absorbance units were used in the analysis. Values of 0.7427, 0.7413, and 0.7435 $cm^3\ g^{-1}$ for the partial specific volumes of AhpF, F[1−202], and F[208−521], respectively, were calculated from the amino acid compositions (*26*). The solvent density, at 1.00942 g $cm^{-3}$, was measured using a DA-310M precision density meter (Mettler Toledo, Hightstown, NJ) thermostated at 20 °C. Theoretical molecular weight values for monomers were obtained using the "Compute pI/$M_W$" tool at http://www.expasy.ch/tools/ (*27*).

*Computational Structure Prediction*. In the present study, protein models were constructed using the following programs: GeneFold and Composer (Tripos Associates, Inc., St. Louis, MO), FFAS (*28*), and Modeller (*29*). The multiple sequence alignment shown in Results was performed using CLUSTAL W available at the Biology Workbench of the San Diego Supercomputer Center (http://workbench.sdsc.edu/) (*30*). While a detailed explanation of these algorithms can be found in their respective references, a brief description of the methodology is given here. In protein structure prediction by modeling there are three crucial steps: recognition of the appropriate template (i.e., the known protein structure that is hypothesized to be similar to the structure of the protein being predicted (the target)), alignment between the target and the template proteins, and building of the model. In modeling based on the structures of close homologues the first two steps are relatively simple (see below for modeling of F[208−521]). However, in the modeling studies described herein for F[1−202], there were no obvious homologues that could be used for modeling. Therefore, we used several approaches that combine both sequence and structure information to recognize appropriate templates among distantly related proteins. Recent structure prediction studies on a variety of proteins that exhibit low sequence similarity to other proteins of known structure clearly show the advantages of using a multitude of approaches in identifying distant evolutionary relationships between proteins (*31*−*34*). In most such cases, sequence comparisons alone were unsuccessful in identifying family connections that could lead to plausible model building. To arrive at more sensitive recognition of distant homologies and better alignments between such proteins, two types of information can be used to enhance the quality of sequence alignments. In one approach, sequences of closely homologous proteins are used to understand varied patterns of allowed mutations along the sequence of both target and template proteins and to derive position-specific mutation matrices. Such matrices allow for much better recognition of similarity between distantly related proteins (*35*). In a second approach, structural information about one of the proteins is used to introduce additional scoring terms based on a possible fit between a prediction target sequence and template structure (*32*). Both approaches were used to identify appropriate template structures for F[1−202] to be used in modeling.

*Structural Modeling*. Structural predictions for AhpF were conducted by breaking up the sequence into N- and C-terminal fragments, each of which was modeled independently. A strong sequence similarity between F[208−521] and TrR can be recognized by almost any sequence alignment method. With 35% sequence identity over a 314 amino acid fragment there is no question that this is an appropriate template. A structural model of the C-terminal fragment of AhpF was built from the GeneFold alignment of F[208−521] to TrR (PDB code 1trb) and refined using tools from the Sybyl suite of molecular modeling programs (Tripos Associates, Inc.). The model was built with the Composer module and in the next step α, amide, and other polar hydrogens were added and proline ring conformations were adjusted where required. Initial minimization (without electrostatics, Tripos force field) was then conducted with the protein backbone constrained to relieve the structure of bad side-chain contacts. All other hydrogens were then added and the model was further minimized with the backbone constrained. After the minimization converged (BGFS algorithm, energy change per step $< 0.001$ kcal $mol^{-1}$), further minimization to convergence was conducted in the absence of constraints. Electrostatics were then slowly introduced over five cycles of convergent minimization (dielectric constant varied in steps of 160, 80, 40, 20, and 2). Finally, the FAD cofactor, taken from the crystal structure of 1trb, was added to the FAD-binding domain of the AhpF model. Side chains lining the FAD-binding cavity were adjusted to relieve bad contacts where necessary.

There are no obvious homologous structural templates to the N-terminal fragment of AhpF preceding the TrR-like fragment modeled as described above. The FFAS method (*28*) was used to match this fragment to a structure of protein disulfide oxidoreductase (PDO) from *Pyrococcus furiosus* (PDB code 1a8l). Despite a low sequence similarity (20.8% sequence identity), FFAS indicated a reliable prediction with a *Z*-score of 58.9. The structural model of the N-terminal fragment of AhpF was created by Modeller using the alignment generated by FFAS and was not further refined.

Analyses of the secondary structure contents of each of the models and of 1tde, the structure file corresponding to

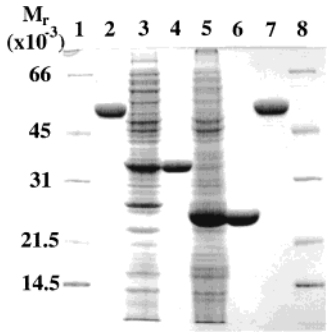


FIGURE 2: SDS−polyacrylamide gel electrophoresis of F[208−521] and F[1−202] proteins expressed in JM109(DE3) before and after purification. Acrylamide gels (12%) were run with samples pretreated by boiling for 3 min in sample buffer containing 2% SDS and 5% 2-mercaptoethanol. The 0.75-mm-thick gels were electrophoresed at 45 mA each in the presence of 1% SDS. Lanes 1 and 8 contain low-range protein standards from BioRad with the indicated $M_r$ values. Lanes 3 and 5 contain 25-$\mu$g samples of the crude *E. coli* extracts from IPTG-induced cultures harboring the pAF[208−521] and pAF[1−202] expression plasmids, respectively. Lanes 4 and 6 contain 8 $\mu$g of the respective purified proteins, and lanes 2 and 7 contain the same amount of intact AhpF.

wild-type TrR, were carried out using DSSP (*36*). Using this program, each residue was assigned to be part of a helix (H for an α helix or G for a 3−10 helix), strand (E), or turn (T), and the total number of each divided by the total number of residues in the structure was taken to be the fraction of the protein containing that secondary structural element.

## RESULTS

*Spectroscopic and Catalytic Properties of Each Independently Expressed Fragment of AhpF, F[1−202] and F[208−521].* Expression of each truncated protein from PCR-generated plasmids (Figure 1) allowed for the purification of each to homogeneity in high yields (Figure 2). The flavin-containing larger fragment of AhpF, F[208−521], was found to possess spectroscopic and catalytic properties identical to those demonstrated previously for the isolated tryptic fragment of AhpF which begins at residue 203 (*3*). The flavin absorption spectrum of F[208−521] (>310 nm) is indistinguishable from that of the wild-type AhpF protein (Poole, 1996); measured values for the flavin content and extinction coefficient at 449 nm for the truncated protein were 1.02 FAD/subunit and 12 900 $M^{-1}$ $cm^{-1}$, respectively. The decreased amino acid-to-flavin ratio effected by the truncation of the protein is reflected in a lower $A_{280}/A_{449}$ ratio for F[208−521] (4.7 compared with 5.4 for intact AhpF). Flavin-dependent transhydrogenase and oxidase activities, which do not require intact redox-active disulfide centers as shown previously for cysteine-to-serine mutants of AhpF (*5*) were very similar for F[208−521] and intact AhpF (Table 1). In contrast, catalysis of NADH-dependent DTNB and AhpC-mediated peroxide reduction was severely hampered by the lack of the N-terminal domain of AhpF (Table 1). The 22 292 Da N-terminal fragment alone, with an extinction coefficient at 279 nm of 15 100 $M^{-1}$ $cm^{-1}$, possesses no chromophoric cofactor and does not itself catalyze electron transfer from NADH.

Circular dichroism (CD) measurements for the two fragments and intact AhpF allowed comparisons of the visible spectra due to bound flavin and the secondary structural content of each as evaluated in the far UV region. The visible CD spectra of intact AhpF and the truncated flavoprotein, F[208−521], indicated small qualitative differences between the structural and electronic environments of the bound FAD in the two proteins (Figure S1 in Supporting Information); similar minor deviations in the visible CD signal for bound flavin were detected for cysteine-to-serine mutants of AhpF studied previously (*5*). Comparisons of CD spectra of each AhpF fragment in the far UV region indicate a much stronger signal, and thus higher α-helical content, for F[1−202] relative to that of F[208−521] (Table 2). To further assess these CD spectra relative to that of the wild-type protein, each signal was multiplied by the number of residues generating it, followed by addition of the two signals and comparison with the intact protein. Although a very small portion of the AhpF protein is not accounted for between the two fragments (residues 203−207), the combined spectra closely resemble the intact AhpF spectrum (Figure S2 in Supporting Information). This observation strongly supports the hypothesis that separately expressed fragments maintain the secondary structure of the native protein.

Table 1: Activities of Intact AhpF and Fragments[a]

| activity | intact AhpF | F[208−521] | F[208−521] + F[1−202] |
|---|---|---|---|
| oxidase[b] | 112 ± 3 | 91.5 ± 1.9 | 91.7 ± 2.6 |
| transhydrogenase[c,d] | 3390 ± 80 | 4330 ± 150 | 4240 ± 120 |
| DTNB reductase[c,e] | 1430 ± 60 | 35.0 ± 1.7 | 35.1 ± 0.4 |
| peroxidase[f] | 8050 ± 226 | 6.0 ± 1.8 | 31.2 ± 8.4 |

[a] Results reported as mean ± standard error expressed as micromoles of substrate reduced per min relative to micromoles of FAD determined at 450 nm; all assays were repeated at least five times, except for the peroxidase assays which were repeated three times. F[1−202] was added in a 1:1 molar ratio with respect to F[208−521] where indicated. [b] Assays performed in 50 mM potassium phosphate buffer at pH 7.5, with 0.5 mM EDTA and 150 $\mu$M NADH, with 30−60 pmol of each protein in a total volume of 1 mL. [c] Activities measured in 50 mM Tris-HCl buffer at pH 8.0, with 0.5 mM EDTA, 100 mM ammonium sulfate, and 150 $\mu$M NADH in a total volume of 1 mL. [d] Included 150 $\mu$M AcPyAD$^+$ and 2.5−7 pmol of protein. [e] Included 500 $\mu$M DTNB (from a 0.1 M stock prepared in DMSO) and 0.7−3 pmol of intact AhpF or 25−100 pmol of truncated protein. [f] AhpF-dependent peroxidase activity was measured anaerobically in 50 mM potassium phosphate buffer at pH 7.0, with 0.5 mM EDTA, 100 $\mu$M ammonium sulfate, 200 $\mu$M NADH, 1 mM cumene hydroperoxide, 0.1 $\mu$M (intact) or 10 $\mu$M (truncated) AhpF, and 20 $\mu$M AhpC; these experiments employed a stopped-flow spectrophotometer for data collection.

Table 2: Secondary Structure Analyses of AhpF and Fragments Based on CD Spectra and Models

| | α helix (or 3−10 helix) | β sheet | turn | total |
|---|---|---|---|---|
| AhpF | | | | |
| model | 31 | 24 | 10 | |
| CD, Varslc1 | 33 | 10 | 12 | 77 |
| CD, Selcon | 34 | 15 | 19 | 101 |
| F[208−521] | | | | |
| model | 29 | 29 | 10 | |
| CD, Varslc1 | 25 | 24 | 16 | 95 |
| CD, Selcon | 32 | 16 | 18 | 101 |
| F[1−202] | | | | |
| model | 35 | 20 | 12 | |
| CD, Varslc1 | 50 | −13 | 4 | 54 |
| CD, Selcon | 48 | 11 | 15 | 100 |

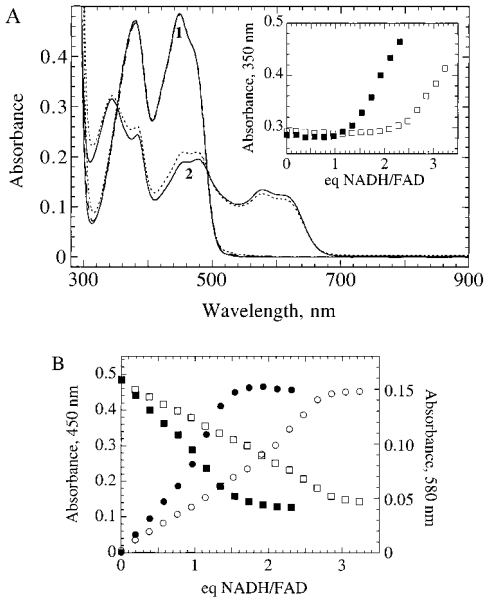


FIGURE 3: Anaerobic NADH titration of F[208−521] in the presence and absence of F[1−202]. F[208−521] (18 nmol) in 25 mM potassium phosphate (pH 7.0) containing 1 mM EDTA and the protocatechuic acid/protocatechuate dioxygenase oxygen-scrubbing system in a total volume of 0.5 mL at 25 °C was made anaerobic and titrated with a 3 mM anaerobic solution of NADH. Panel A shows oxidized spectra (1) of F[208−521] in the absence (solid line) and presence (dotted line) of F[1−202], compared with intact AhpF (dashed line). Spectra of reduced proteins (2) were taken after the addition of 1.35 and 2.47 equiv of NADH, respectively, to F[208−521] in the absence (solid line) and presence (dotted line) of F[1−202]. The inset of panel A shows the absorbance changes at 350 nm during the titration; intersection of the linear portions of these absorbance changes (near the isosbestic point for FAD and FADH•) indicates oxidation of 1.4 and 2.4 equiv of NADH/FAD, respectively, for F[208−521] in the absence and presence of F[1−202] (compared with 2.6 equiv of NADH/FAD for intact AhpF) (*3*). Panel B depicts the absorbance changes at 450 (squares) and 580 nm (circles) during the titration. Symbols in panels A and B represent F[208−521] in the absence (closed symbols) and presence (open symbols) of F[1−202].

*Electron-Transfer Interactions within and between the Two Fragments of AhpF.* Anaerobic reductive titrations of F[208−521] with dithionite (not shown) or NADH (Figure 3) result in spectral changes essentially identical to those seen for the wild-type enzyme (*3*), except that approximately 1 equiv less dithionite or NADH per flavin is consumed during the titration. The disulfide center of F[1−202] also retains its redox activity in the presence of F[208−521]; when added in a stoichiometric amount to F[208−521] prior to titration with NADH, the disulfide center of F[1−202] restores the endpoint of NADH oxidation to approximately that seen for the wild-type enzyme (Figure 3). The free thiol concentration following each titration also confirms the NADH-dependent reduction of the Cys129−Cys132 disulfide center in F[1−202] (4.1 versus 6.0 thiols/FAD for F[208−521] in the absence and presence, respectively, of F[1−202]). Interestingly, spectral changes on reduction of the flavin-containing fragment (F[208−521]) are reversible on addition of excess AhpC; following dithionite titrations (which contain 1/100 equiv of methyl viologen), the pseudo-first-order rate of F[208−521] reoxidation is about 20-fold higher in the presence of equimolar F[1−202] than in its absence. This result strongly supports the proposed role for the N-terminal region of AhpF in mediating the transfer of electrons between Cys345−Cys348 and AhpC (*3, 5*).

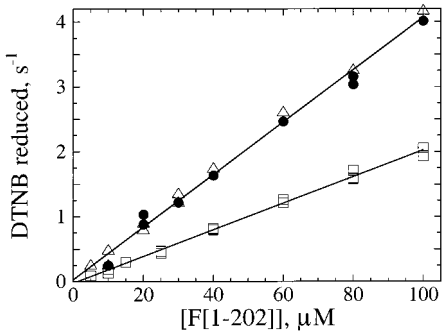


FIGURE 4: DTNB-linked assay of F[1−202] reduction by F[208−521] and TrR. Substrates (NAD(P)H and DTNB) in one syringe were mixed with proteins (F[208−521] or TrR and F[1−202]) in the other in a stopped-flow spectrophotometer; rates of increase in $A_{412}$ were measured between 10 and 20 s after mixing. Experiments included DTNB at 0.5 mM (open symbols) or 1.0 mM (closed symbols) and 200 $\mu$M of either NADH (circles and triangles) or NADPH (squares); also included (all given as final concentrations) were 0.5 $\mu$M F[208−521] (circles and triangles) or TrR (squares) and 0−100 $\mu$M F[1−202]. Assay solutions contained 50 mM Tris-HCl at pH 8.0, 0.5 mM EDTA, and 100 mM ammonium sulfate; assays were conducted at 25 °C. Data have been corrected for rates of DTNB reduction in the absence of F[1−202] which were 0.6 and 1.0 s$^{-1}$ at 0.5 and 1.0 mM DTNB, respectively, for F[208−521] and 0.14 s$^{-1}$ at 0.5 mM DTNB for TrR.

Assays performed using standard conditions indicate no change in the oxidase, transhydrogenase, or DTNB reductase activities of F[208−521] in the presence of a stoichiometric amount of F[1−202], and only a small increase in the anaerobically measured peroxidase activity with AhpC (Table 1). A significant degree of DTNB reduction was observed, however, when F[1−202] was included in greater amounts. Using DTNB as a reporter of electron transfer to F[1−202], we were able to demonstrate a linear dependence of the rate of TNB production on the concentration of F[1−202] when the latter was varied from 5 to 100 $\mu$M in the presence of 0.5 $\mu$M F[208−521] (Figure 4). The second-order rate constant for electron transfer between the two fragments, 4.0 $\times$ 10$^4$ M$^{-1}$ s$^{-1}$, was independent of the concentration of DTNB added; at 0.5 $\mu$M F[208−521] and 100 $\mu$M F[1−202], DTNB reduction occurred at about one-fourth the rate of that with 0.5 $\mu$M intact AhpF. When the experiment was performed in standard peroxidase assay buffer at pH 7.0 (without peroxide) rather than in the DTNB reductase assay buffer used in the above experiment, the rate of interprotein electron transfer, at about 3 $\times$ 10$^4$ M$^{-1}$ s$^{-1}$, was not increased. A further test of intermolecular electron transfer was carried out using the C129,132S mutant of AhpF in place of F[208−521]. This mutant showed the same linear dependence on F[1−202] concentration but exhibited an 8-fold lower rate of electron transfer to F[1−202] (data not shown).

*Substrate Specificity of F[208−521] and TrR.* Given the homology between the C-terminal portion of AhpF and full-length TrR from *E. coli*, we tested for the capacity of either intact AhpF or F[208−521] to catalyze NADH-dependent Tr reduction. TrR activity was not detected in either protein using standard DTNB- and insulin-linked assays and *E. coli* Tr. We then pursued anaerobic pyridine nucleotide titrations of Tr in the presence of 1/100 molar amounts of the

flavoprotein to be tested as we had done previously with AhpC (Figure 3 in ref *3*). In the presence of TrR, additions of NADPH up to 1 equiv relative to Tr resulted in essentially no change in $A_{340}$, whereas further additions of NADPH did not result in oxidation of the added pyridine nucleotide and therefore gave the expected rise in $A_{340}$. Similar NADH titrations of Tr in the presence of F[208−521] alone or in combination with F[1−202] did not result in detectable oxidation of the pyridine nucleotide, suggesting no reduction of Tr. In another approach, an 8-fold excess of reduced pyridine nucleotide over Tr was added anaerobically in the presence of 1/100 molar amounts of TrR, F[208−521], or F[208−521] plus F[1−202], and aliquots were taken over time for thiol assays with DTNB under denaturing conditions. Full reduction accounting for 2.1 −SH/subunit of Tr was detected in the TrR-containing sample as rapidly as the sample could be taken after the pyridine nucleotide addition (∼30 s). Reduction of Tr by F[208−521] in the presence of excess NADH was exceedingly slow but detectable by this method; after 20 h about one-third of the Tr was reduced. Pseudo-first-order rate comparisons indicated that F[208−521] reduced Tr at least 5−6 orders of magnitude more slowly than did TrR. Intact AhpF transferred electrons to Tr at half the rate of F[208−521], and addition of F[1−202] to F[208−521] in these experiments had no effect on the electron-transfer rate. Thus, AhpF lacking the N-terminus is not an effective TrR.

The capacity for TrR to reduce F[1−202] was also explored using the DTNB assays described above for F[208−521]. Under identical conditions (except with 200 $\mu$M NADPH rather than NADH), TrR was nearly as effective a reductant of F[1−202] as was F[208−521], giving a bimolecular rate constant of about $2 \times 10^4$ $M^{-1}$ $s^{-1}$ (Figure 4).

*AhpC Reduction by Fragments of AhpF: Use of an Engineered Fluorophore-Linked AhpC Substrate.* Peroxidase activity with AhpC was very low (and difficult to measure) in the presence of one or both fragments of AhpF (Table 1), apparently due to the slow transfer of electrons between the two fragments as shown by DTNB assays (Figure 4). Therefore, we designed a new AhpC substrate containing a fluorophore linked, via a disulfide bond, to Cys165 of the C46S mutant of AhpC (*4*, *37*). This construct, designated AhpC-FAM, proved to be an excellent substrate for intact AhpF; $k_{cat}$ and $K_m$ values of 25.5 ± 1.1 $s^{-1}$ and 14.3 ± 1.9 $\mu$M, respectively (determined by monitoring NADH oxidation spectroscopically), were about 9-fold and 1.4-fold lower than wild-type AhpC values (*38*), indicating a decrease in catalytic efficiency of just 7-fold with this substrate.

Evaluation of the ability of F[208−521] to reduce AhpC-FAM at substrate concentrations of 14.4 and 29 $\mu$M (at and above the $K_m$ determined by using intact AhpF) gave a rate of fluorophore release less than 0.1% of that with intact AhpF at the given concentrations. To assess the rate of reaction of F[1−202] with AhpC-FAM, F[1−202] was first reduced by a 100-fold excess of dithiothreitol and isolated from free reagent by gel filtration chromatography. Reduced F[1−202] generated in this way gave a thiol content of 2.05 mol of SH/mol of protein as determined with DTNB; the reduced protein is highly stable in air. F[1−202] was then mixed aerobically with excess AhpC-FAM in the stopped-flow spectrofluorometer. Fluorescence changes were readily fit to a single exponential at each concentration of AhpC-FAM;

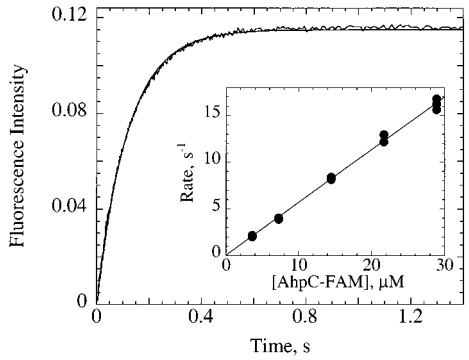


FIGURE 5: Reduction of AhpC-FAM by reduced F[1−202]. F[1−202] (0.35 $\mu$M) prereduced with dithiothreitol was mixed with AhpC-FAM at varying concentrations in peroxidase assay buffer (50 mM potassium phosphate, pH 7.0, with 0.5 mM EDTA and 100 $\mu$M ammonium sulfate) at 25 °C in the stopped-flow spectrophotometer. Shown are the fluorescence changes observed on mixing reduced F[1−202] with 14.4 $\mu$M AhpC-FAM and the fitted single-exponential curve. The inset shows the pseudo-first-order rates of fluorescence change observed over varying concentrations of AhpC-FAM up to 29 $\mu$M.

Table 3: Sedimentation Equilibrium Analyses of AhpF, F[208−521], and F[1−202]

| | theoretical $M_W$ | | $M_W$ from sedimentation equilibrium |
|---|---|---|---|
| | monomer | dimer | |
| AhpF | 56 735 | 113 469 | 107 400 ± 2 100 |
| F[208−521] | 34 137 | 68 273 | 68 800 ± 1 600 |
| F[1−202] | 22 292 | 44 584 | 21 820 ± 900 |

a replot of the pseudo-first-order rate constants versus the concentration of AhpC-FAM indicated an effectively irreversible second-order reaction between reduced F[1−202] and AhpC-FAM with a rate constant of $1.2 \times 10^6$ $M^{-1}$ $s^{-1}$ (Figure 5). This rate constant is nearly identical to the catalytic efficiency measured by steady-state assays using intact AhpF ($1.8 \times 10^6$ $M^{-1}$ $s^{-1}$), establishing that the N-terminus of AhpF, not the C-terminal region, plays a direct role in AhpC reduction during turnover.

*Subunit Composition of Wild-Type and Truncated AhpF Proteins by Analytical Ultracentrifugation.* One goal of these studies has been to make structural and functional comparisons of AhpF with TrR using both empirical and predictive methods in the absence of high-resolution structural information from X-ray diffraction or NMR data. Therefore, we used sedimentation equilibrium analyses to characterize the oligomerization state of each of the proteins under investigation. Analyses of individual data sets at a variety of concentrations and speeds yielded molecular weight values that exhibited no significant dependence on either protein concentration or rotor speed, consistent with the single ideal species model (*25*). Global fits of the data to this model (Figure S3 in Supporting Information) resulted in the weight-average molecular weight ($M_W$) values shown in Table 3. Data recorded at 450 nm for intact AhpF and F[208−521] gave a slightly lower $M_W$ value in the former case (at 98 400 ± 2000) and were not included in the global analyses. Our results clearly indicated that, like TrR, AhpF is a dimer in solution at these concentrations. Furthermore, F[208−521] is also dimeric, whereas F[1−202] is monomeric under these conditions (up to 130 $\mu$M). These results support a model in which the dimer interface of AhpF lies largely

Table 4: Sequence Alignment for Residues 208−521 of AhpF (Third Line) and Residues 1−316 of the C138S Mutant of *E. coli* TrR (Fourth Line), Including Secondary Structure Calculated for the AhpF Model (Second Line) and Secondary Structure Calculated for 1trb (Fifth Line)[a]

```
        10         20         30         40         50         60         70         80
  EEEEEEEEE   HHHHHHHHHHHHTT   EEE-   TTTGGGG  EE   TT   E-EHHHHHHHHHHHHHTT EE
NKRDAYDVLIVGSGPAGAAAAVYSARKGIRTGLM-GERFGGQVLDTVDIENYISVPKT-EGQKLAGALKAHVSDYDVDVI
GTTKHSKLLILGSGPAGYTAAVYAARANLQPVLITGMEKGGQLTTTTEVENWPGDPNDLTGPLLMERMHEHATKFETEII
  EEEEEEEEE   HHHHHHHHHHHTTT   EEE    TTGGGGG       TT      HHHHHHHHHHHHHTT EEE
              o       +  + +                     + oo++++      o  +o  +  +

        90        100        110        120        130        140        150        160
       EEEEE     EEEEETTEEEEEEEEEEE   EEE     HHHHHT TTTEE  HHHHGGGGTT EEEEE   H
DSQSASKLVPAATEGGLHQIETASGAVLKARSIIIATGAKWRNMNVPGEDQYRTKGVTYCPHCDGPLFKGKRVAVIGGGN
FDH----INKVDLQNRPFRLNGDNGEYT-CDALIIATGASARYLGLPSEEAFKGRGVSACATSDGFFYRNQKVAVIGGGN
   ----EEEEE    EEE EE   EEE-EEEEEE   EEE     HHHHHT TTTEE  HHHHGGGGTT EEEEE   H
                                                              ++

       170        180        190        200        210        220        230        240
HHHHHHHHHHHH  EEEEE         HHHHHHH-THHHH  EE --  EEEEEEE    EEEEEEE  TT  - EEEE
SGVEAAIDLAGIVEHVTLLEFAPEMKADQVLQDKV-RSLKNVDIIL--NAQTTEVKGDGSKVVGLEYRDRVSGD-IHSVA
TAVEEALYLSNIASEVHLIHRRDGFRAEKILIKRLMDKVENGNIILHTNRTLEEVTGDQMGVTGVRLRDTQNSDNIESLD
HHHHHHHHHTTT  EEEEE         HHHHHHHHHHHHT  EEEE   EEEEEEE    EEEEEEE  TT    EEEE
          +                        +   +

       250        260        270        280        290        300        310        320
  EEEE   EEE  GGGTTT  EETTEE      -----     TTEEE  TTT      HHHHHHHHHHHHHHHHHHH
LAGIFVQIGLLPNTHWLEGALERNRMGEIIIDAK-----CETSVKGVFAAGDCTTVPYKQIIIATGEGAKASLSAFDYLIRTKIA
VAGLFVAIGHSPNTAIFEGQLELEN-GYIKVQSGIHGNATQTSIPGVFAAGDVMDHIYRQAITSAGTGCMAALDAERYLDGL---
  EEEE   EEE  GGGTTT  EET-TEE         TTB   TTEEE GGGG      HHHHHHHHHHHHHHHHHHHTT
                       +        +  +  +                  +   o  o        + +   +
```

[a] In lines two and five, H = alpha helix, E = extended strand, T = hydrogen-bonded turn, G = 3−10 helix; symbols in the sixth line identify residues in TrR involved in stabilization of the dimer interface through hydrophobic (○) or other (+) interactions. The box highlights the position of catalytic cysteine residues in AhpF and the C138S mutant of TrR.

within the C-terminal part of the molecule.

*Modeling of the C-Terminus of AhpF*. Evidence that the C-terminal and N-terminal fragments are independently folding portions of AhpF possessing functional and structural properties similar to those in the intact protein provided a basis for our pursuit of the modeling of AhpF in two parts. Using GeneFold, 1trb (the structure file corresponding to the C138S mutant of TrR) was by far the best template for modeling of F[208−521]; other high-scoring matches included FAD/NAD(P)-binding proteins within the same family. The alignment of TrR with F[208−521] (Table 4) depicts the conservation of amino acid residues critical for redox function (CPHC and CATS at positions 140−143 in the alignment for AhpF and TrR, respectively) and cofactor binding (e.g., GXGXXg/a motifs underlined at positions 12−17 and 157−162 in the alignment) between the two proteins. On the other hand, residues identified in the TrR structure as participating in H-bonding, electrostatic, or hydrophobic interactions within the dimer interface are only moderately conserved (Table 4). Of a total of 24 residues involved in H-bonding interactions across the dimer interface of TrR, only six are identical in AhpF (Figure 6). In some cases, however, side-chain differences would not be likely to affect intersubunit interactions (e.g., where backbone atoms are the H-bonding partners). One electrostatic interaction in TrR (between Asp55 and Arg67′) which is apparently missing in AhpF may be replaced by a new interaction between Lys263 and Asp279′ in AhpF. Six of seven residues identified as the hydrophobic core of the TrR dimer interface are also hydrophobic in AhpF. Thus, the packing of the dimer interface of AhpF is likely to be quite similar to that of TrR, although small differences in specific interactions between residues in different subunits are expected. Most notable in our model of F[208−521] (Figure 6) are the distinct upper (pyridine nucleotide binding) and lower (flavin binding) domains tethered by two $\beta$ meanders which, in TrR, have been proposed to provide the flexibility needed for large structural rotations between the two domains (*9*). Such flexibility may be required for alternating interactions between redox centers in AhpF as well, as described in the discussion.

Comparison of the secondary structural contents from the model of F[208−521] (Figure 6) and those estimated from the CD spectrum (182−260 nm; Figure S2 in Supporting Information) gives a very reasonable agreement between the two (Table 2). Using these same analyses, the α-helical, $\beta$-sheet, and turn contents of TrR (at 28, 27, and 10%, respectively, from 1tde, the structure file corresponding to wild-type TrR) were best approximated from the CD spectrum (C. M. Reynolds and L. B. Poole, unpublished) using the Varslc1 program (at 32, 27, and 13%, versus 33, 19, and 26% for Selcon). Varslc1 analyses accounted for 95% of the total CD signal for F[208−521] and 93% of the signal for TrR, but only 77% of the total signal for intact AhpF (Table 2).

*Modeling of the N-Terminus of AhpF*. The FFAS algorithm identified a structural template with statistically significant similarity to F[1−202]: a protein disulfide oxidoreductase

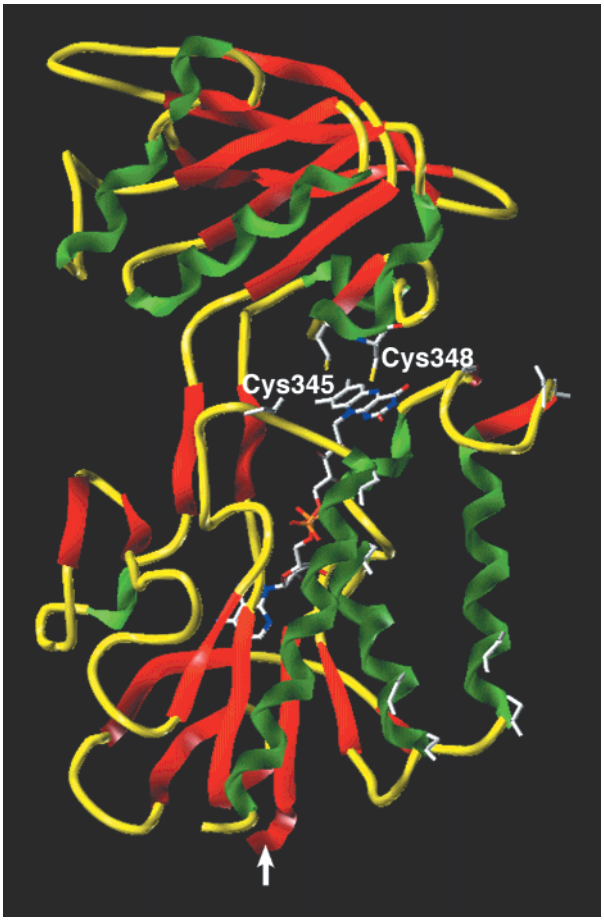


FIGURE 6: Structural model of F[208−521]. The structure of residues 209−516 of AhpF predicted by GeneFold (Tripos Associates, Inc.) using 1trb (the structure file for the C138S mutant of TrR) as the template is depicted by a ribbon diagram of the backbone atoms and thick lines to represent structures of Cys345 and Cys348 (linked to the upper, pyridine nucleotide-binding domain) and of FAD (noncovalently bound to the lower, flavin-binding domain). The FAD structure used in the model was taken directly from the known structure of this cofactor in 1trb. Secondary structural elements as recognized by the program DSSP (*36*) are shown in green (α and 3−10 helices) and red (*β* sheets). The location of the attachment point for the remaining N-terminal residues of AhpF is shown by the arrow at the bottom. Backbone atoms of eight absolutely conserved residues corresponding to dimer interface residues of TrR and two new putative salt-bridging residues in AhpF (Lys 263 at the upper right and Asp279 at the lower right of the flavin-binding domain) are shown in white. This figure was generated using the Molecular Graphics program SYBYL (Tripos Asso., Inc.).

(PDO) from *Pyrococcus furiosis* with two Tr-like folds, each containing a functional CXXC motif (*39*). Despite a low (20.8%) sequence identity between F[1−202] and PDO, the FFAS reliability score indicated a strong match with a *Z*-score of 58.9. In extensive tests of the FFAS algorithm on a large benchmark, no false positive was found with a *Z*-score higher than 7 (*28*). A further verification of this prediction is that the FFAS algorithm independently matched a Tr structure (PDB code 2trxB) to residues 100−202 of AhpF with a *Z*-score of 10.2 and to residues 1−100 of AhpF with a *Z*-score of 6.8. Interestingly, our studies have indicated that proteins containing multiple Tr repeats are ubiquitous (A. Godzik, unpublished).

The structure-based sequence alignment of PDO and F[1−202] generated by FFAS clearly indicates the correspondence of the CXXC active site of F[1−202] with that in the C-terminal Tr-like fold of PDO, although the more N-terminal CXXC found in PDO is missing from F[1−202] (Tables 5 and 6). The active-site structure including the more C-terminal CXXC of PDO has a less strained disulfide bond conformation compared to the more N-terminal active-site disulfide bond, consistent with the behavior of the N-terminus of AhpF as a disulfide reductase rather than as a disulfide oxidoreductase involved in disulfide rearrangement or thiol oxidation (*39*). Also noteworthy is the conservation of two glycine residues (Gly80 and Gly184 in AhpF) and of two *cis*-proline residues (Pro63 and Pro172 in AhpF) located on loops opposite their respective active-site CXXC centers in PDO; these residues are thought to play a role in substrate binding (Table 6). The apparent gene duplication event that has led to the creation of a unique two-Tr fold (not characterized as two separate domains in PDO because of their close packing) in both PDO and AhpF may have occurred more than once in evolution or may indicate the divergence of these protein "modules" from a common ancestor.

Comparison of the secondary structural contents from the model of the N-terminus of AhpF (Figure 7) and those estimated from the CD spectra (182 to 260 nm; Figure S2 in Supporting Information) was more problematic due to the relatively poor fit of the spectra by the secondary structure estimation programs. Varslc1, which was the better estimation program when used to compare the CD spectral analyses with the known secondary structure content from the X-ray crystal structure of TrR (see above), gave a negative content for both antiparallel and parallel *β*-sheet content and a total of only 54% of the spectrum accounted for (Table 2). Selcon may be the better program in this case, but it is not clear how well this estimation program characterizes the CD spectrum of this fragment of AhpF. All methods indicate a higher α-helical content in this part of the protein than in the C-terminus. This expectation of a high helical content for the F[1−202] fragment is reasonably well satisfied by the model depicted in Figure 7.

*Modeling of Intact AhpF*. Because of the lack of knowledge about how the two parts of AhpF associate, construction of a detailed model of intact AhpF was not actively pursued. Without detailed knowledge about the structure and linkage of the N-terminal domain to the rest of the molecule, it is, nonetheless, possible to make a prediction regarding the path of electron transfer between domains of AhpF. The attachment of the N-terminal domain to the rest of the polypeptide occurs at the end of the flavin domain distant from the pyridine nucleotide domain (arrow at the bottom of Figure 6). The head-to-tail arrangement of the dimers suggests closer proximity of Cys129−Cys132 in the N-terminal domain to the other redox-active disulfide center, Cys345′−Cys348′, in the pyridine nucleotide-binding domain of the other subunit. The functional significance of this prediction is that electron transfer between redox-active disulfide centers in the N-terminal and C-terminal parts of AhpF would be expected to occur across subunits, and monomeric enzyme would be inactive. Experiments are underway to test these predictions, and further information can be expected when a high-resolution structural model of AhpF becomes available.

Table 5: Sequence Alignment for Residues 1−199 of AhpF (Third Line) and Residues 6−225 of *Pyrococcus furiosus* Protein Disulfide Oxidoreductase (Fourth Line), Including Secondary Structure Calculated from the Model of AhpF (Second Line) and Secondary Structure Calculated for 1a8l (Fourth Line)[a]

```
         10        20        30        40        50        60        70        80
   HHHHHHHHHTT      EEEEEEE    -------  HHHHHHHH   EEEEEEETT TTTTT -------   EEE
MLDTNMKTQLRAYLEKLTKPVELIATLDDSA-------KSAEIKELLAEIAELSDKVTFKEDNTLPV-------RKPSFL
--DADKKVIKEEFFSKMVNPVKLIVFVRKDHCQYCDQLKQLVQELSELTDKLSYEIVDFDTPEGKELAKRYRIDRAPATT
--HHHHHHHHHHTGGG    EEEEEEE     TTHHHHHHHHHHHHHTT TTEEEEEEETT HHHHHHHHHTT     EEE

        90       100       110       120       130       140       150       160
EE TT    EEEE    TTHHHHHHHHHHHHHH      HHHHHHHTT    EEEEEEE    TTHHHHHHHHHHHHHH
ITNPGSQQGPRFAGSPLGHEFTSLVLALLWTGGHPSKEAQSLLEQIRDIDGDFEFETYYSLSCHNCPDVVQALNLMAVLN
ITQDGKDFGVRYFGLPAGHEFAAFLEDIVDVSREETNLMDETKQAIRNIDQDVRILVFVTPTCPYCPLAVRMAHKFAIEN
EEETT    EEEE    TTHHHHHHHHHHHHHHT     HHHHHHHTT    EEEEEEE    TTHHHHHHHHHHHHHHH

       170       180       190       200       210       220
-----TTEEEEEEETTT HHHHHHTT     EEE--     --       HHHHHHHHHHHH
-----PRIKHTAIDGGTFQNEITERNVMGVPAVF--VNGKE--FGQGRMTLTEIVAKVDTGA
TKAGKGKILGDMVEAIEYPEWADQYNVMAVPKIVIQVNGEDRVEFEGAYPEKMFLEKLLSAL
HHTT   EEEEEEEGGG HHHHHHTT     EEEEEETTEEEEEEE    HHHHHHHHHHHH
```

[a] Secondary structure designations as in Table 4. Boxes highlight the positions of catalytic cysteine residues.

Table 6: Multiple Sequence Alignment of Each Tr-like Region of AhpF and *Pyrococcus furiosus* Protein Disulfide Oxidoreductase (PDO) with *E. coli* Tr and *E. coli* Glutaredoxin-1 (Glx1) Protein Sequences[a]

```
PDOnt          MGLISDADKKVIKEEFFSKMVNPVKLIVFVRKDHCQYCDQLKQLVQELS-ELTDKLSYEI
AhpFnt1        ---MLDTNMKTQLRAYLEKLTKPVELIATL--DDSAKSAEIKELLAEIA-ELSDKVTFKE
PDOct          -----ETNLMDETKQAIRNIDQDVRILVFVT-PTCPYCPLAVRMAHKFA-IENTKAGKGK
Tr             --MSDKIIHLTDDSFDTDVLKADGAILVDFWAEWCGPCKMIAPILDEIADEYQGKLTVAK
Glx1           ----------------------MQTVIFGR-SGCPYCVRAKDLAEKLS-NERDDFQYQY
AhpFnt2        -----PSKEAQSLLEQIRDIDGDFEFETYYS-LSCHNCPDVVQALNLMA-VLNPRIKHTA


PDOnt          VDFDTPEGKEL---AKRYRIDRAPATTITQDGKDFGVRYFGLPAGHEFAAFLEDIVDVSRE
AhpFnt1         -DNTLP----------VRK---PSFLITNPGSQQGPRFAGSPLGHEFTSLVLALLWTGGH
PDOct          ILGDMVEAIEYPEWADQYNVMAVPKIVIQVNGEDR-VEFEGAYPEKMFLEKLLSALS---
Tr             LNIDQNPGT-----APKYGIRGIPTLLLFKNGEVA-ATKVGALSKGQLKEFLDANLA---
Glx1           VDIRAEGITK----EDLQQKAGKPVETVPQIFVDQ--QHIGGYTD--FAAWVKENLDA--
AhpFnt2         IDGGTFQN-E----ITERNVMGVPAVFVNGKEFGQ-----GRMTLTEIVAKVDTGAEKR-
                                          *               *
```

[a] The box highlights the position of catalytic cysteine residues. Asterisks denote fully conserved residues. Sequences shown are residues 1−117 and 118−226 for PDO (PDOnt and PDOct, respectively), residues 1−100 and 101−202 for AhpF (AhpFnt1 and AhpFnt2, respectively), and full length Tr and Glx1.

## DISCUSSION

Our evaluation of truncated fragments of AhpF corresponding to the region with TrR homology (F[208−521]) and the "appended" N-terminal domain (F[1−202]), now recognized to contain a double Tr-like fold, has been a powerful tool in analyses of structural features, and ultimately of the catalytic roles, of each of these regions of the AhpF protein. The location of a "hinge" region connecting the two parts of AhpF, around Ala203, was previously suggested by the location of a tryptic sensitive site; on digestion, the C-terminus remains largely intact while the N-terminus is hydrolyzed to yield much smaller fragments (*3*). Our characterization of a similar C-terminal fragment reported herein, based on independent expression of the portion of AhpF which aligns with TrR (residues 208−521), has indicated no difference between F[208−521] and the tryptic fragment described previously (*3*).

Assessment of structural features of the two fragments of AhpF indicates preservation of at least some of the corresponding features of the intact protein. The far UV circular dichroism spectra of the two fragments, when summed, give a spectrum strikingly similar to that of the intact protein, thereby suggesting preservation of essentially all of the AhpF secondary structural elements in the truncated versions of the protein. CD spectral features also support a high α-helical content for F[1−202] relative to that for F[208−521]. Sedimentation equilibrium analyses of AhpF and the two independently expressed fragments support the location of a dimer interface wholly or largely within the C-terminal part of AhpF, consistent with significant domain movement that is hypothesized to occur during N-terminus-mediated electron transfer between the Cys345−Cys348 dithiol of AhpF and Cys46−Cys165′ of AhpC (*3*, *37*). Predictive methods strongly support topological homology between

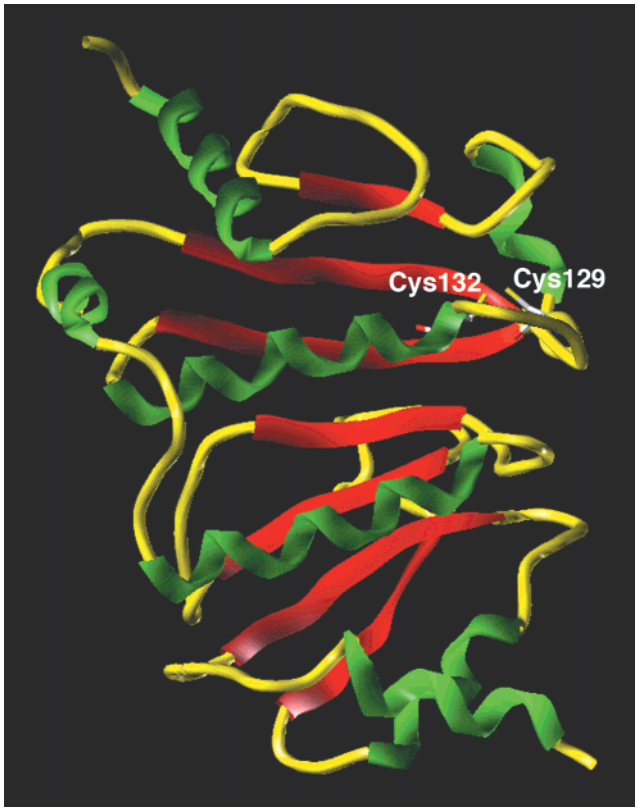


FIGURE 7: Structural model of F[1−202]. The structure of residues 1−202 of AhpF predicted by FFAS and Modeller using 1a8l (the structure file for PDO) as the template is depicted as in Figure 6. The two half-cystine residues of the redox-active disulfide center are shown as thick lines.

dimeric TrR and the C-terminus of AhpF. The N-terminal domain of AhpF is also predicted to contain two tandem Tr-like folds as has been demonstrated for PDO, but lacks one of the two functional CXXC motifs present in the latter protein.

Functional comparisons of the truncated proteins with intact AhpF have been particularly illuminating in terms of the role each part plays in catalysis. Only the N-terminus of AhpF is capable of rapid AhpC reduction, fully supporting our view that the role of the Cys129−Cys132 disulfide center, and the domain which contains it, is to transfer electrons between the dithiol form of Cys345−Cys348 (the TrR-like disulfide center) and the intersubunit active-site disulfide bond of AhpC. That the N-terminus of AhpF can be viewed as a redox domain similar to Tr, but covalently attached to its electron donor, is also supported by these findings. It is notable, however, that electron transfer between the two parts of AhpF is quite slow when they are not attached (more than 2 orders of magnitude slower than the $k_{cat}/K_m$ value for intact AhpF interacting with AhpC). The slow interaction between these two parts of AhpF when they are in separate molecules is not just a result of an altered structure for the flavin-containing part in the absence of the N-terminus; C129,132S, with an intact structure (to the best of our knowledge) but no N-terminal redox center, is even less active in electron transfer to F[1−202]. These results strongly argue against intermolecular electron transfer between AhpF dimers during catalytic turnover. Modeling of the AhpF dimer does, however, support the possibility that intersubunit electron transfer, occurring between the reduced Cys345−Cys348 center of one subunit and the oxidized Cys129−Cys132 center of the other, is required for catalysis. Experiments are underway to firmly establish the path of electron transfer within the AhpF dimer.

Our demonstration of the direct participation of both disulfide redox centers and bound flavin of AhpF in electron transfer from NADH to AhpC highlights the rapidity with which these multiple electron transfers and putative structural rotations must occur; $k_{cat}$ for AhpF turnover at 25 °C is greater than 200 $s^{-1}$ (*38*). In fact, rapid reaction kinetic studies of a homologue of *S. typhimurium* AhpF, the NADH oxidase of *Amphibacillus xylanus*, have indicated that flavin reduction is rate-limiting in the reduction of this protein by 2 equiv of NADH; electron transfer from $FADH_2$ to the C-terminal disulfide center (and perhaps on to the N-terminal disulfide center) must therefore occur at a rate much greater than 200 $s^{-1}$ at 25 °C (*40*). In these studies, a slow step in enzyme reduction (0.5 $s^{-1}$) associated with partial oxidation of a third equivalent of NADH was interpreted as the reduction of $EH_4$ to $EH_6$ limited by electron transfer between the C-terminal and N-terminal dithiol/disulfide redox centers. Our studies reporting the direct participation of the N-terminal redox center in catalysis of AhpC reduction by AhpF, if translatable to the *A. xylanus* NADH oxidase/AhpC system as we would expect, indicate that electron transfer between the C-terminal and N-terminal redox-active disulfide centers must be fast enough to support catalysis. The apparently differing results between the two types of experiments on these homologues could be reconciled as follows. $EH_6$ of *A. xylanus* NADH oxidase need not be a catalytically important species. Furthermore, $EH_4$ formed on reduction of this enzyme with NADH may also include a partially or fully reduced N-terminal redox center as described below for AhpF.

Considerations of the multiple domain interactions and electron transfers which must occur during catalysis by AhpF have led us to propose the cycling of this enzyme between $EH_2$ and $EH_4$ redox states during rapid catalytic turnover (*16*, *37*). During "priming" of the enzyme by the first equivalent of NADH, two electrons would be passed to the flavin, and then to the C-terminal disulfide center following a conformational change (Figure 8). The catalytic cycle would then require one conformational change to allow for reduction of FAD by the next NADH substrate molecule and simultaneous transfer of two electrons from Cys345−Cys348 to Cys129−Cys132 (generating species **5** and **6** of Figure 8), followed by one more conformational change to permit re-reduction of Cys345−Cys348 by $FADH_2$ and concomitant electron transfer from Cys129−Cys132 to AhpC (generating species **7** and **4** of Figure 8). Such a mechanism includes the direct mediation of the N-terminal domain in electron transfer and takes maximal advantage of each conformational change to accomplish the necessary electron transfers. Our mechanism also includes the intersubunit electron-transfer hypothesized to occur on the basis of structural considerations (see above).

*S. typhimurium* AhpF and *A. xylanus* NADH oxidase are clearly complex flavoproteins with multiple redox centers; it is noted, however, that the appendage of additional protein sequences at the N- or C-termini of the "core" structure of disulfide reductases related to glutathione reductase has been observed in several other cases, as well. Mercuric ion

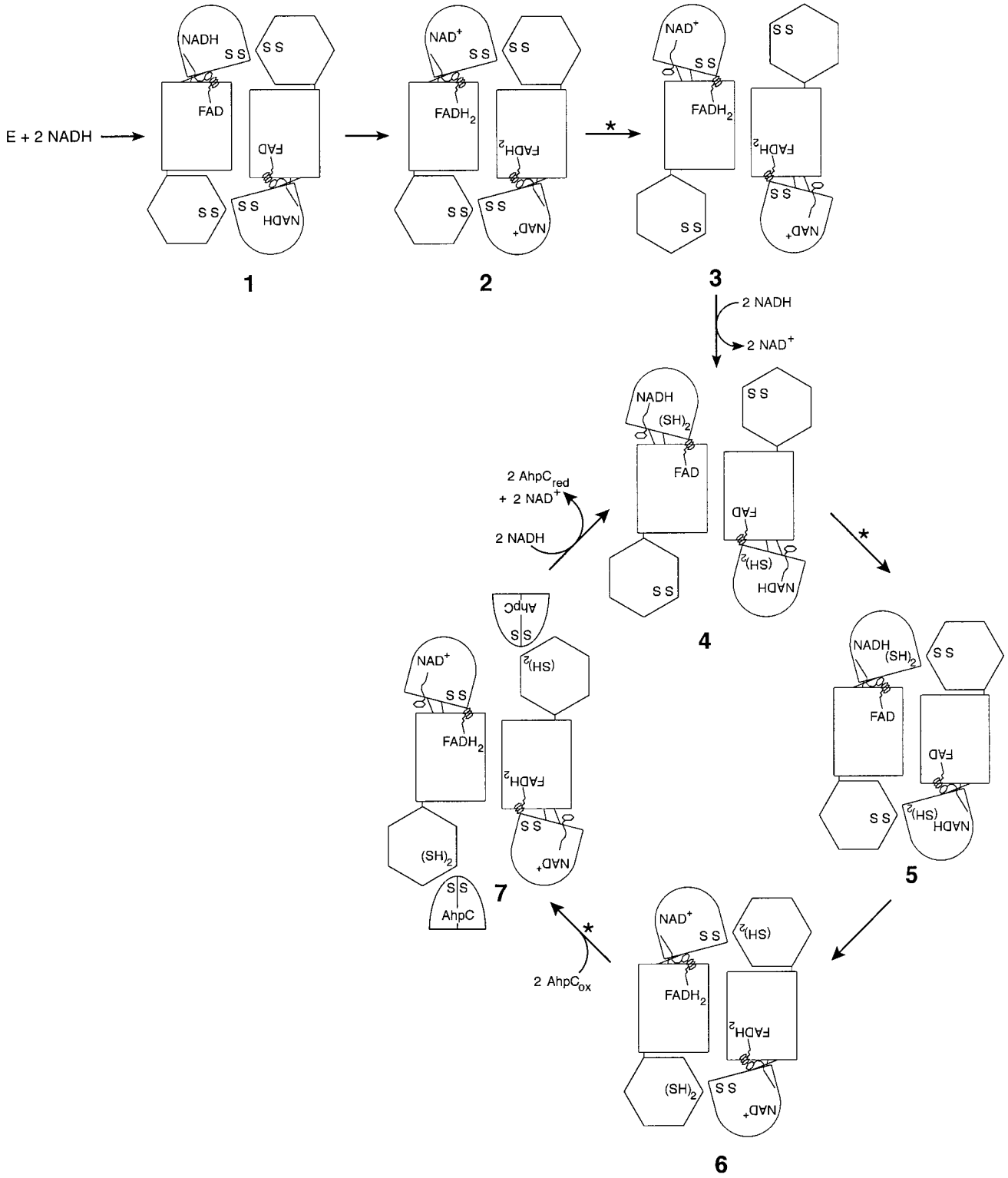


FIGURE 8: Hypothesized priming and turnover of AhpF in the presence of excess NADH and AhpC. AhpF is depicted as a "head-to-tail" dimer. The pyridine nucleotide-binding domain (bell shape) is shown with NADH or $NAD^+$ bound (the nicotinamide ring is represented by the small hexagon) and an oxidized (SS) or reduced [$(SH)_2$] Cys345−Cys348 redox center. The isoalloxazine ring of FAD (or $FADH_2$) bound to the flavin-binding domain (rectangle) is represented by the three attached hexagons. The disulfide center (Cys129−Cys132) in the N-terminal domain of AhpF (large hexagon) is also depicted in its oxidized (SS) or reduced [$(SH)_2$] form. The simplified priming and turnover steps are depicted as synchronous events in each part of the dimer (two turnovers per dimer per cycle). During priming, binding and electron transfer from NADH to FAD (species **1** and **2**) are followed by a conformational change (asterisk) which then allows for reduction of the Cys345−Cys348 disulfide center in the pyridine nucleotide-binding domain of AhpF by the flavin (species **3** and **4**). Species **4**, a two-electron-reduced form of AhpF ($EH_2$), is also depicted with NADH having displaced the $NAD^+$ product as might be expected in the presence of excess NADH. Catalytic turnover (species **4**−**7**) includes the hypothesized intersubunit electron transfer occurring between species **5** and **6** and two conformational changes (asterisks) per cycle. AhpC is depicted as half of a dimer (half-ellipse) with a single active site in either the oxidized (SS; $AhpC_{ox}$) or reduced ($AhpC_{red}$) form. Actual proton transfers and ionization states are not intended to be accurate in this scheme. See Discussion for details.

reductase, for example, has an additional disulfide redox center at the N-terminus and another cysteine pair at the C-terminus with a role in metal binding (*41*−*43*). The high-molecular-weight TrR from humans also contains an additional redox center, composed of one cysteine and a selenocysteine, located at its C-terminus (*44*, *45*). Interestingly, a fused TrR and Tr protein expressed in *Mycobacterium leprae* has recently been identified (*46*, *47*). Although in the *M. leprae* "fusion" protein the smaller Tr redox component is attached at the C-terminus of TrR rather than at the N-terminus (as with AhpF), this architecture need not be very different from that of AhpF as the C- and N-termini of TrR are located very close to one another at the end of the FAD domain opposite the NADP(H) domain (α carbons of Lys7 and Leu313 are 8.1 Å apart in the crystal structure) (*9*). Both parts of the *M. leprae* fusion protein, TrR and Tr, are functional, although the TrR portion has been shown to exhibit inherently slow catalytic turnover relative to that of the *E. coli* TrR (*47*). Whether or not electron transfer between TrR and Tr in this fusion protein is an intra- or intermolecular process remains unresolved.

## SUMMARY

The N-terminal 202 amino acids with a tandem repeat of Tr-like folds and the TrR-like C-terminus of AhpF are separately folding functional units of the protein. Intermolecular electron transfer between these fragments, and presumably between dimers of intact AhpF, is slow relative to catalysis. The catalytic role of the N-terminus of AhpF is to transfer electrons from the C-terminal part of AhpF to the intersubunit active-site disulfide bond of AhpC for ultimate reduction of cellular hydroperoxides.

## ACKNOWLEDGMENT

The authors thank Charles Williams, Jr., for his generous gift of *E. coli* Tr and TrR used in early studies, C. Michael Reynolds for construction of overexpression vectors and purification of TrR for later studies, Lois LaPrade and Jennifer Nixon for assistance with protein purifications, and Chris Ashwell and Yi-Dan Wang for construction of the pAF[208−521] and pAF[1−202] expression vectors, respectively.

## SUPPORTING INFORMATION AVAILABLE

Additional information includes figures depicting the visible CD spectra for F[208−521] and AhpF (Figure S1), the far UV CD spectra of F[1−202], F[208−521], and AhpF (Figure S2), and the sedimentation equilibrium data for F[1−202], F[208−521], and AhpF (Figure S3). This material is available free of charge via the Internet at http://pubs.acs.org.

## REFERENCES

1. Jacobson, F. S., Morgan, R. W., Christman, M. F., and Ames, B. N. (1989) *J. Biol. Chem. 264*, 1488−1496.
2. Poole, L. B., and Ellis, H. R. (1996) *Biochemistry 35*, 56−64.
3. Poole, L. B. (1996) *Biochemistry 35*, 65−75.
4. Ellis, H. R., and Poole, L. B. (1997) *Biochemistry 36*, 13349−13356.
5. Li Calzi, M., and Poole, L. B. (1997) *Biochemistry 36*, 13357−13364.
6. Chae, H. Z., Robison, K., Poole, L. B., Church, G., Storz, G., and Rhee, S. G. (1994) *Proc. Natl. Acad. Sci. U.S.A. 91*, 7017−7021.
7. Tartaglia, L. A., Storz, G., Brodsky, M. H., Lai, A., and Ames, B. N. (1990) *J. Biol. Chem. 265*, 10535−10540.
8. Williams, C. H., Jr. (1995) *FASEB J. 9*, 1267−1276.
9. Waksman, G., Krishna, T. S. R., Williams, C. H., Jr., and Kuriyan, J. (1994) *J. Mol. Biol. 236*, 800−816.
10. Petsko, G. A. (1991) *Nature 352*, 104−105.
11. Russel, M., and Model, P. (1988) *J. Biol. Chem. 263*, 9015−9019.
12. Wang, P.-F., Veine, D. M., Ahn, S. H., and Williams, C. H., Jr. (1996) *Biochemistry 35*, 4812−4819.
13. Lennon, B. W., Williams, C. H., Jr., and Ludwig, M. L. (1997) in *Flavins and Flavoproteins 1996* (Stevenson, K. J., Massey, V., and Williams, C. H., Jr., Eds.) pp 713−716, University of Calgary Press, Calgary, Alberta, Canada.
14. Mulrooney, S. B., and Williams, C. H., Jr. (1997) *Protein Sci. 6*, 2188−2195.
15. Veine, D. M., Ohnishi, K., and Williams, C. H., Jr. (1998) *Protein Sci. 7*, 369−375.
16. Poole, L. B. (1997) in *Flavins and Flavoproteins 1996* (Stevenson, K. J., Massey, V., and Williams, C. H., Jr., Eds.) pp 751−760, University of Calgary Press, Calgary, Alberta, Canada.
17. Gally, D. L., Rucker, T. J., and Blomfield, I. C. (1994) *J. Bacteriol. 176*, 5665−5672.
18. Toumadje, A., Alcorn, S. W., and Johnson, W. C. J. (1992) *Anal. Biochem. 200*, 321−331.
19. Sreerama, N., and Woody, R. W. (1993) *Anal. Biochem. 209*, 32−44.
20. Prongay, A. J., Engelke, D. R., and Williams, C. H., Jr. (1989) *J. Biol. Chem. 264*, 2656−2664.
21. Luthman, M., and Holmgren, A. (1982) *Biochemistry 21*, 6628−6633.
22. Bailey, J. L. (1962) *Techniques in Protein Chemistry*, pp 294−295, Elsevier Scientific Publishing Co., Inc., New York.
23. Bradford, M. M. (1976) *Anal. Biochem. 72*, 248−254.
24. Yphantis, D. A. (1964) *Biochemistry 3*, 297−317.
25. Johnson, M., Correia, J. J., Yphantis, D. A., and Halvorson, H. (1981) *Biophys. J. 36*, 575−588.
26. Laue, T. M., Shah, B. D., Ridgeway, T. M., and Pelletier, S. L. (1992) in *Analytical Ultracentrifugation in Biochemistry and Polymer Science* (Harding, S. E., Rowe, A. J., and Horton, J. C., Eds.) pp 90−125, The Royal Society of Chemistry, Cambridge.
27. Wilkins, M. R., Gasteiger, E., Bairoch, A., Sanchez, J.-C., Williams, K. L., Appel, R. D., and Hochstrasser, D. F. (1998) in *2-D Proteome Analysis Protocols* (Link, A. J., Ed.), Humana Press, Totowa, NJ.
28. Rychlewski, L., Jaroszewski, L., Li, W., and Godzik, A. (2000) *Protein Sci. 9*, 232−241.
29. Sali, A., and Blundell, T. L. (1993) *J. Mol. Biol. 234*, 779−815.
30. Thompson, J. D., Higgins, D. G., and Gibson, T. J. (1994) *Nucleic Acids Res. 22*, 4673−4680.
31. Rychlewski, L., Zhang, B., and Godzik, A. (1999) *Protein Sci. 8*, 614−624.
32. Jaroszewski, L., Rychlewski, L., Zhang, B., and Godzik, A. (1998) *Protein Sci. 7*, 1431−1440.
33. Fischer, D., and Eisenberg, D. (1997) *Protein Sci. 5*, 947−955.
34. Rice, D., and Eisenberg, D. (1997) *J. Mol. Biol. 267*, 1026−1038.
35. Brenner, S. E., Chothia, C., and Hubbard, T. J. (1998) *Proc. Natl. Acad. Sci. U.S.A. 95*, 6073−6078.
36. Kabsch, W., and Sander, C. (1983) *Biopolymers 22*, 2577−2637.
37. Poole, L. B. (1999) in *Flavins and Flavoproteins 1999* (Ghisla, S., Kroneck, P., Macheroux, P., and Sund, H., Eds.) pp 691−694, Agency for Scientific Publications, Berlin.
38. Poole, L. B., Higuchi, M., Shimada, M., Li Calzi, M., and Kamio, Y. (2000) *Free Radical Biol. Med. 28*, 108−120.

39. Ren, B., Tibbelin, G., de Pascale, D., Rossi, M., Bartolucci, S., and Ladenstein, R. (1998) *Nat. Struct. Biol. 5*, 602−611.
40. Niimura, Y., Ohnishi, K., Nishiyama, Y., Kawasaki, S., Miyaji, T., Suzuki, H., Nishino, T., and Massey, V. (1997) in *Flavins and Flavoproteins 1996* (Stevenson, K. J., Massey, V., and Williams, C. H., Jr., Eds.) pp 741−750, University of Calgary Press, Calgary, Alberta, Canada.
41. Walsh, C. T., DiStefano, M. D., Moore, M. J., Shewchuk, L. M., and Verdine, G. L. (1988) *FASEB J. 2*, 124−130.
42. Moore, M. J., Miller, S. M., and Walsh, C. T. (1992) *Biochemistry 31*, 1677−1685.
43. Engst, S., and Miller, S. M. (1998) *Biochemistry 37*, 11496−11507.
44. Gladyshev, V. N., Jeang, K. T., and Stadtman, T. C. (1996) *Proc. Natl. Acad. Sci. U.S.A. 93*, 6146−6151.
45. Arscott, L. D., Gromer, S., Schirmer, R. H., Becker, K., and Williams, C. H., Jr. (1997) *Proc. Natl. Acad. Sci. U.S.A. 94*, 3621−3626.
46. Wieles, B., van Noort, J., Drijfhout, J. W., Offringa, R., Holmgren, A., and Ottenhoff, T. H. (1995) *J. Biol. Chem. 270*, 25604−25606.
47. Wang, P.-F., Marcinkeviciene, J., Williams, C. H., Jr., and Blanchard, J. S. (1998) *Biochemistry 37*, 18378−18389.

BI000405W